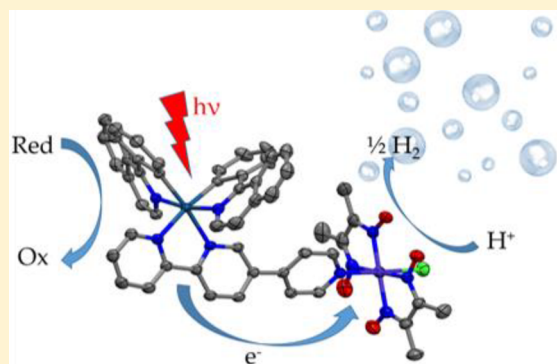


Photocatalytic Hydrogen Production Using a Red-Absorbing Ir(III)–Co(III) Dyad

Cédric Lentz,[†] Olivier Schott,[‡] Thomas Auvray,[‡] Garry Hanan,^{*,‡} and Benjamin Elias^{*,†}[†]Institute of Condensed Matter and Nanosciences, Molecules, Solids and Reactivity, Université catholique de Louvain, Place Louis Pasteur 1, 1348 Louvain-la-Neuve, Belgium[‡]Département de Chimie, Université de Montréal, 2900 Boulevard Edouard-Montpetit, Montréal, Québec H3T 1J4, Canada

Supporting Information

ABSTRACT: The synthesis of a Ir(III)–Co(III) dyad with vectorial electron transfer afforded a novel supramolecular system that photocatalytically produces hydrogen in a range extending from the blue region of the spectrum to the red region with higher turnover number and frequency compared to other bimetallic dyads.

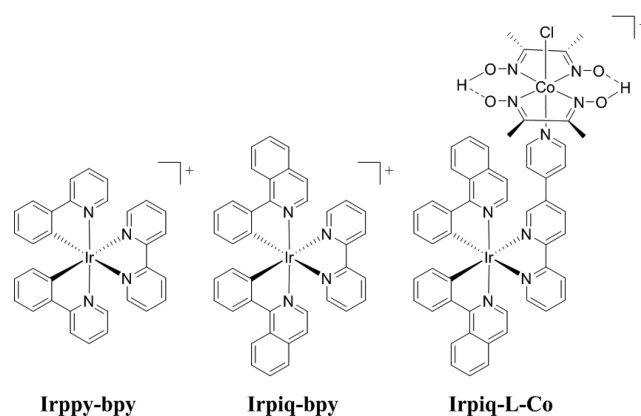


INTRODUCTION

With the view of developing a sustainable energy supply, molecular hydrogen is a promising fuel.^{1–6} A sunlight-triggered hydrogen evolution reaction (HER) would be an interesting solution to the worldwide consumption of fossil fuels because hydrogen is a noncarbon source of alternative energy.⁷ HER is typically based on photoinduced electron transfer from a photosensitizer (PS) to a catalytic center, where hydrogen is produced.^{8,9} Such a process requires efficient charge separation via vectorial electron transfer, and covalent and robust assemblies are also highly recommended.^{10–12} Many of the studies reported so far use transition-metal complexes as PSs and transition-metal derivatives as catalysts.^{13–21} Co complexes are widely used as catalysts for HER because they show considerable improvement for electro- and photocatalysis compared to later transition metals.^{22–30} Cobaloxime appears to be one of the most studied molecular catalysts because of its simple synthesis and high efficiency.^{31,32} For instance, cobaloxime moieties have been tethered to Pt(II), Re(I), Ru(II), and Ir(III) PS complexes.^{14,15,33} With respect to HER, covalent linkage of the PS to the catalyst gives, in general, enhanced hydrogen production compared to dissociated, bimolecular systems,^{14,34} despite some exceptions, e.g., with zinc porphyrin systems.^{35–37} More recently, in our group, several Ir(III)–Co(III) dyads have been developed and were shown to photoevolve hydrogen upon green-light irradiation.³³ In terms of photophysical and electrochemical tunability, Ir(III) complexes are excellent candidates for the development of robust and efficient supramolecular coordination assemblies for HER. In these assemblies, the archetypical bidentate [Ir(ppy)₂(bpy)]⁺ (termed hereafter Irppy-bpy) motif is often used

because it shows high stability and enhanced efficiency compared to other transition-metal complexes. In this work, we present a new Ir–Co dyad for HER that is efficiently working at longer irradiation wavelengths including yellow and red light. The dyad Irpiq-L-Co (Chart 1) displays cyclometalated piq ligands (where piqH is 1-phenylisoquinoline), with enhanced conjugation with respect to ppy ligands (where ppyH is 2-phenylpyridine) inducing a higher and red-shifted molar absorption. Furthermore, the ancillary ligand L (where L is 2,2';5',4'-terpyridine) connects the PS unit to the Co(III)

Chart 1. Structure of Bis-cyclometalated Ir(III) Complexes Used for HER



Received: March 23, 2017

catalyst, allowing vectorial electron transfer. Substitution on the 4 or 5 position of 2,2'-bipyridine (bpy) did not give significant differences in the properties of the complexes. Control systems, i.e., Irppy-bpy (or Irpiq-bpy), coupled to [Co(dmgH)₂PyCl] (where dmgH is dimethylglyoximate) are described as well to compare the efficiency of mono- and multicomponent Ir(III)–Co(III) systems.

Synthesis of the dyad Irpiq-L-Co was achieved by replacing a chloro ligand from [Co(dmgH)(dmgH₂)Cl₂] (where dmgH₂ is dimethylglyoxime) by the pendant pyridine of the trischelate complex Irpiq-L (see the Supporting Information). Crystals suitable for X-ray diffraction were obtained by the slow diffusion of diisopropyl ether into an acetonitrile solution of Irpiq-L-Co at room temperature (Figure 1). The Ir

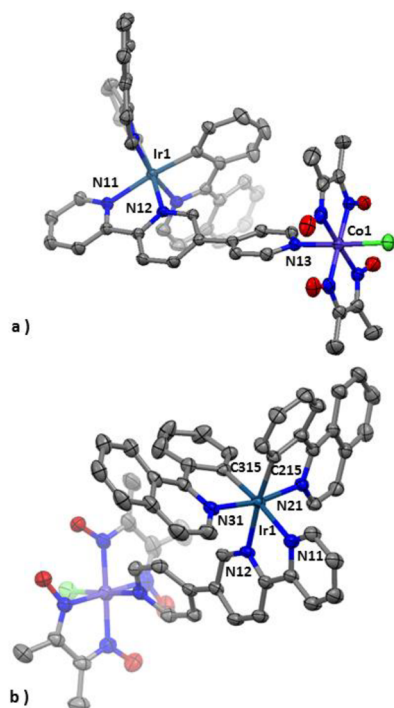


Figure 1. X-ray structure of Irpiq-L-Co: (a) view of the terpyridine-bridging ligand; (b) view of the Ir coordination sphere. Ellipsoid at the 50% probability level. H atoms, PF₆ counteranions, and cocrystallized solvent molecules are omitted for clarity.

coordination sphere in Irpiq-L-Co does not differ significantly from those previously reported for Irppy-bpy³⁸ and Irpiq-bpy³⁹ (Table S5). The twist angle between the pendant pyridine and the coordinated bpy moiety of L is approximately 31° and corresponds to that reported for Ru³⁴ or Ir³³ derivatives. The same angle was found to be around 34° in the optimized geometry of Irpiq-L modeled by density functional theory (DFT), using an acetonitrile continuum. The tethered cobaloxime geometry is similar to that of the free cobaloxime, as observed for other Ir–Co dyads.³³ The two components maintain their own distinct properties upon association in the supramolecular dyad.

To better understand the electronic interaction between the two components in the dyad, its electrochemical properties were measured using cyclic voltammetry and compared to those of reference compounds. The oxidation and reduction potentials of Irpiq-L-Co and the other PSs are gathered in Table 1, and voltammograms are displayed in Figures S9–S16.

Table 1. Electrochemical Data^a of Irppy-bpy, Irpiq-bpy, Irpiq-L, and Irpiq-L-Co in Acetonitrile

	Irppy-bpy	Irpiq-bpy	Irpiq-L	Irpiq-L-Co
E_{ox}	+1.37 (129)	+1.36 (156)	+1.43 (irr)	+1.43 (irr)
E_{red}	–1.30 (111)	–1.30 (128), –1.67 (104)	–1.09 (124), –1.60 (173), –1.75 (131)	–0.43 (irr), –0.95 (71), –1.09 (75), –1.55 (110), –1.73 (77)

^aPotentials are given in volts vs Ag/AgCl. The electrochemical data were measured with 0.1 M Bu₄NClO₄ at 100 mV s^{–1} with a complex concentration of 10^{–4} mol L^{–1}. For reversible waves, the differences between the anodic and cathodic peak potentials (mV) are given in parentheses. irr = irreversible.

Regarding the mononuclear complexes, the slightly more positive oxidation potential of the Ir centers containing L instead of bpy (1.43 vs 1.36 V) can be attributed to the increased back-bonding to the extended 2,2';5',4''-terpyridine ligand L. The same explains the less negative first reduction wave (–1.09 vs –1.30 V) and is confirmed by DFT calculations showing that the lowest unoccupied molecular orbital (LUMO) is centered on the N[^]N ligand in all cases (Tables S6–S8). Except Irppy-bpy, all complexes display a reduction wave at ~–1.7 V vs Ag/AgCl, which is attributed to the reduction of the isoquinoline moieties.

Irpiq-L-Co displays an irreversible one-electron reduction wave at –0.43 V vs Ag/AgCl corresponding to the reduction of Co(III) to Co(II). The irreversibility of the process is explained by the loss of the chloride ion from the Co center upon one-electron reduction.⁴⁰ A subsequent reversible reduction of Co(II) in Co(I) can be observed at –0.95 V vs Ag/AgCl. It is worth mentioning that reduction values of the Ir–Co dyad are slightly less negative compared to the parent complexes Irpiq-L and [Co(dmgH)₂PyCl] ($E_{\text{red}} = -1.10$ V vs Ag/AgCl in MeCN) because of the electron-withdrawing character of both metal centers in the assembly compared to separate compounds.⁴¹

Figure 2 displays the absorption and emission spectra for Irpiq-L-Co and the related PSs (values are gathered in Table S1) in acetonitrile. All of the complexes display intense absorption bands in the UV region ($\epsilon > 10^4$ M^{–1} cm^{–1} under 340 nm) tailing into the visible. It is worth mentioning that the

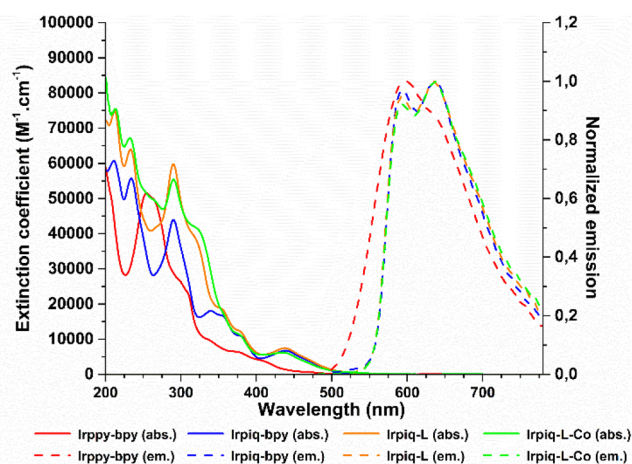


Figure 2. Absorption and emission spectra of Irpiq-L-Co and the Ir(III) PSs Irppy-bpy, Irpiq-bpy, and Irpiq-L in CH₃CN at room temperature.

absorption spectra of Irpiq-L-Co and Irpiq-L are almost identical, showing that no strong electronic interaction occurs between the metallic centers of the dyad. Because of the higher conjugation of the cyclometalated piq ligands compared to ppy, Irpiq complexes display more intense absorption bands in the visible region than Irppy-bpy with an intense absorption band centered at 438 nm ($\epsilon \sim 7 \times 10^3 \text{ M}^{-1} \text{ cm}^{-1}$). Furthermore, the absorption bands for these complexes extend further than 525 nm, with contributions from $^1\text{MLLCT}$ [metal/ligand-to-ligand charge transfer; $d\pi(\text{Ir}-\text{C}) \rightarrow \pi^*(\text{N}^{\wedge}\text{N})$], $^1\text{MLCT}$ [metal-to-ligand charge transfer; $d\pi(\text{Ir}) \rightarrow \pi^*(\text{C}^{\wedge}\text{N})$], $^3\text{MLCT}$ [$d\pi(\text{Ir}) \rightarrow \pi^*(\text{C}^{\wedge}\text{N})$], and $^3\text{MLLCT}$ [$d\pi(\text{Ir}-\text{C}) \rightarrow \pi^*(\text{N}^{\wedge}\text{N})$] states according to time-dependent DFT (TD-DFT) calculations (see Tables S6–S11), matching what was previously reported for the corresponding Ir(III) PSs.⁴²

Interestingly, Irpiq-L-Co shows a residual emission close to the emission of the parent PS Irpiq-L in acetonitrile, indicating that coordination of Co(III) does not lower the LUMO of the dyad, in agreement with the similar reduction potential of the N[^]N ligand with or without Co. Nevertheless, the lower lifetime and quantum yield of the dyad compared to the separate units imply an intramolecular electron transfer from the excited Ir(III) unit to the Co(III) unit, yet not with 100% efficiency. Consequently, a major contribution of the Co(III) center to the LUMO of the dyad, confirmed by the reduction potential of Co(III)–Co(II), is considered, and residual emission thus only results from LUMO+1, i.e., centered on the N[^]N ligand of the resulting dyad. Similar observations have been made by Sakai et al. with Ru–Pt dyads, in which efficient hydrogen photoproduction is still observed.²⁷ The emission spectrum for both Irpiq-L-Co and Irpiq-L display structural features, implying a mixed contribution of the ^3LC (ligand-centered) and $^3\text{MLCT}$ excited states, referred to as $^3\text{MLLCT}$, combined to $^3\text{LLCT}$ (ligand-to-ligand charge-transfer) excited states.³⁹

The spectroscopic and electrochemical data suggest that Irpiq-L-Co is an ideal candidate to evolve molecular hydrogen under irradiation. First, photoinduced electron transfer occurs from the cyclometalated Ir fragment toward the terpyridine ligand through population of the $^3\text{MLLCT}$ excited state, with the electron then being transferred to the Co catalyst. Furthermore, with extended absorption tailing up to 600 nm, Irpiq-L-Co should allow hydrogen photoproduction to occur at low energy. At this stage, it should also be mentioned that hydrogen photoproduction via a reductive pathway, i.e., photoreduction of the excited Ir(III), which, in turn, leads to hydrogen production, cannot be fully excluded. Further detailed mechanistic studies are currently under investigation.

The Irpiq-L-Co dyad was tested for photocatalytic hydrogen evolution. As control experiments, Irpiq-bpy and Irppy-bpy, without pendant pyridyl rings, were also tested with free $[\text{Co}(\text{dmgH})_2\text{PyCl}]$ in the same molar ratio to compare the activity of the dissociated systems in the same set of conditions. All photoreactions were performed in acetonitrile with 0.5 M triethanolamine as the sacrificial electron donor and 0.05 M aqueous tetrafluoroboric acid as the proton source; the error associated with the TOF and TON values is 10%. Acetonitrile was chosen as a polar solvent to solubilize the dinuclear complex and to better align our results with previous studies. Other polar but less coordinated solvents could also be used.⁴³ Four different types of light-emitting diodes (LEDs) centered at 452, 525, 595, and 630 nm, respectively (see Figure S18),

were used to study the dependence of the rate of hydrogen evolution at various irradiation wavelengths.^{33,34,44}

For piq derivatives, extension of conjugation on a cyclometalated ligand leads to a red-shifted absorption that requires particular attention at longer wavelengths of irradiation (see Table S1). Under blue irradiation, all PSs are efficiently excited, and the photoredox process triggers hydrogen production (see Table S3). The reference system Irppy-bpy/ $[\text{Co}(\text{dmgH})_2\text{PyCl}]$ quickly reaches a TOF_{max} of $4400 \text{ mmol}_{\text{H}_2} \text{ mol}^{-1} \text{ min}^{-1}$, followed by a rapid degradation to attain a modest TON of 30 after 30 min. The Irpiq-bpy/ $[\text{Co}(\text{dmgH})_2\text{PyCl}]$ system behaves differently. It reacts slowly even under blue-light irradiation: a TOF_{max} of $370 \text{ mmol}_{\text{H}_2} \text{ mol}^{-1} \text{ min}^{-1}$ is attained, but the activity is more sustainable, yielding a TON of 70 after 7 h. Irpiq-L-Co is clearly superior, with a maximum rate of activity of $16000 \text{ mol}_{\text{H}_2} \text{ mol}^{-1} \text{ ps} \text{ min}^{-1}$ and a final TON of 180 after 2.3 h (see Figure S19).

With green irradiation, the overlap of the absorption spectra of the PSs and the emission spectra of the LED is smaller. As a result, the activity is lower. For the dissociated system Irppy-bpy/ $[\text{Co}(\text{dmgH})_2\text{PyCl}]$, a rapid decomposition occurs, resulting in a TON of only 16 after 4 h (Figure 3). Irpiq-bpy/

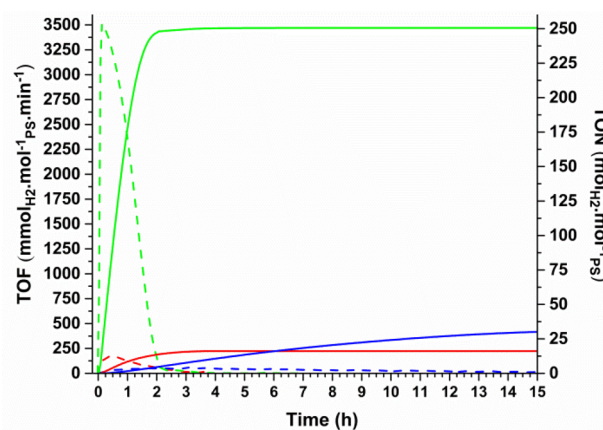


Figure 3. Hydrogen evolution of 0.1 M Irpiq-L-Co (green) in CH_3CN and dissociated systems 0.1 M Irpiq-bpy/ $[\text{Co}(\text{dmgH})_2\text{PyCl}]$ (1/1; blue) and 0.1 M Irppy-bpy/ $[\text{Co}(\text{dmgH})_2\text{PyCl}]$ (1/1; red) in CH_3CN with 0.5 M TEOA as the electron source and 0.05 M HBF_4 as the proton source: solid line, TON; dashed line, TOF. Irradiation centered at 523 nm, green light.

$[\text{Co}(\text{dmgH})_2\text{PyCl}]$ is less active than that under blue irradiation, reaching a TON of 30 after 22 h. Irpiq-L-Co was again highly active with a TOF_{max} of $3500 \text{ mmol}_{\text{H}_2} \text{ mol}^{-1} \text{ ps} \text{ min}^{-1}$ to reach a TON of 251 after 3 h (Figure 3). This performance using green is superior to that of the Ru–Pt system of Sakai et al., which displayed a TON of 4.8 after 10 h.⁴⁴ A rapid degradation of the cobaloxime in the Irpiq-L-Co system after 2 h was confirmed by the addition of a free dmgH_2 ligand.

Using a yellow LED, the dissociated systems are no longer photoactive, while Irpiq-L-Co generates a TON of 180 after 18 h with a TOF_{max} of $270 \text{ mmol}_{\text{H}_2} \text{ mol}^{-1} \text{ ps} \text{ min}^{-1}$ (Figure S20), which follows the slightly lower photon flux for yellow-light irradiation (Table S2). From the absorption profile of Irpiq-L-Co, we anticipated that hydrogen evolution could occur upon red-light irradiation as well (Figure S21). Indeed, Irpiq-L-Co exhibits a somewhat low but nonnegligible hydrogen photo-

production ($\text{TOF}_{\text{max}} = 15 \text{ mmol}_{\text{H}_2} \text{ mol}^{-1}_{\text{PS}} \text{ min}^{-1}$) sustained for 110 h, yielding a TON of 80 (Figure 4), although it is not as

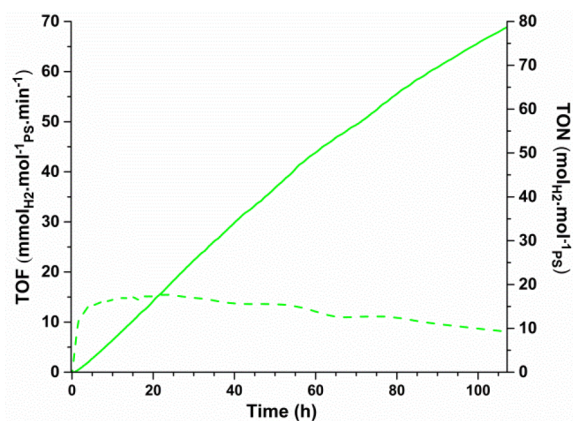


Figure 4. Hydrogen evolution of 0.1 M Irpiq-L-Co in CH_3CN with 0.5 M TEOA as the electron source and 0.05 M HBF_4 as the proton source: solid line, TON; dashed line, TOF. Irradiation centered at 630 nm, red light.

efficient as a recently published Ru–Co₆ system with a TON of 380 after 20 h using red light.³⁴ Our system is, however, more robust than the above system, functioning out past 100 h. Such production with monocomponent systems under red light compared to the inertness of the dissociated system confirms the assessment that intramolecular electron transfer is favored.

CONCLUSION

A new covalent dinuclear system based on a tris-bidentate Ir(III) cationic PS and a cobaloxime catalyst has been prepared and characterized. Overall, the results show that the covalent dyad is more efficient than the corresponding dissociated systems and allows hydrogen photoevolution under low-energy irradiation. The better performance of the dyad compared to the dissociated system can be attributed to spatial interaction between the PS and catalyst through a coordination bond that enhances electronic transfer and stabilizes the system.^{33,34,45} Indeed, enhancing the probability of electron transfer from the reduced PS to the catalyst will lower the probability of decomposition via ligand dissociation.⁴⁶ The stability of the dinuclear compound is close to that of the reported Ir–Co dyad in the literature;^{14,33} however, Irpiq-L-Co is the first Ir–Co dyad to promote yellow- and red-light-driven hydrogen photoproduction.

EXPERIMENTAL DETAILS

¹H NMR experiments were performed on a Bruker AM-500 (500 MHz) spectrometer. The chemical shifts (given in ppm) were measured versus the residual peak of the solvent as the internal standard. Structures and ¹H NMR attributions of the complexes are displayed in the Supporting Information. High-resolution mass spectrometry (HRMS) spectra were recorded on a Q-Exactive orbitrap from ThermoFisher. Samples were ionized by electrospray ionization (ESI; capillary temperature = 250 °C, vaporizer temperature = 250 °C, and sheath gas flow rate = 20). UV–visible absorption spectra were recorded on a Shimadzu UV-1700 spectrometer. Room temperature fluorescence spectra were recorded on a Varian Cary Eclipse spectrometer. Complexes were excited at 400 nm. Luminescence lifetimes were measured with a modified Applied Photophysics laser kinetic spectrometer by exciting the samples with a Nd:YAG pulsed laser (Continuum NY 61-10). Emitted light as a

function of time was detected with a R-928 Hamamatsu photomultiplier tube whose output was applied to a digital oscilloscope (Hewlett-Packard HP 54200A) interfaced with a Dell Dimension DE051 computer. Signals were averaged over at least 16 shots and corrected for baseline. Igor 6.1 software was used for the decay analysis. Cyclic voltammetry was carried out in a one-compartment cell, using a glassy carbon disk working electrode (approximate area = 0.03 cm²), a platinum wire counter electrode, and an Ag/AgCl reference electrode. The potential of the working electrode was controlled by an Autolab PGSTAT 100 potentiostat through a PC interface. The cyclic voltammograms were recorded with a sweep rate of 100 mV s⁻¹ in dried acetonitrile (Acros, HPLC grade). Tetrabutylammonium perchlorate (0.1 M) was used as the supporting electrolyte, and the samples were purged by Ar before each measurement.

X-ray Diffraction. Crystals suitable for X-ray diffraction analysis were obtained by the slow diffusion of diisopropyl ether in an acetonitrile solution of Irpiq-L-Co at room temperature. Two morphologies of crystals were observed (block for structure 1 and needle for structure 2), resulting in the two space groups *P21/n* and *C2/c* (see Table S4). Structure 1 is based on a better quality data set, and it was therefore chosen to discuss the structural parameters of Irpiq-L-Co. Data were collected using a Bruker SMART diffractometer equipped with an APEX II CCD detector, an Incoatec IMuS source, using Cu K α radiation ($\lambda = 1.54178 \text{ \AA}$), and a Quazar MX mirror. The crystal-to-detector distance was 4.0 cm, and data collection was carried out in a 512 × 512 pixel mode. The initial unit cell parameters were determined by a least-squares fit of the angular setting of strong reflections, collected by a 180.0° scan in 180 frames over three different parts of the reciprocal space. The structure was solved by intrinsic phasing using the program SHELX^{47,48} and refined on *F*² by full-matrix least squares using SHELXL.^{47,48} The non-H atoms were refined anisotropically, using weighted full-matrix least squares on *F*². Mainly H atoms are treated as riding atoms using SHELXL^{47,48} default parameters. Only H atoms implicated in the hydrogen-bonding pseudomacrocyclic of the cobaloxime were placed, and the chemical occupancy was fixed to 0.5 for each of four protons. The disorder of the position of the PF₆ anion was treated by modeling two positions that were refined with free variable occupancy. High residual electronic densities were assimilated to disordered solvent molecules (diisopropyl ether and/or acetonitrile). Modeling the identification and organization of the solvent was unsuccessful. They were removed using the SQUEEZE routine from PLATON.⁴⁹ As a result, an improvement of the *R*₁ factor with ~2.6% was obtained. A solvent-accessible void of 2228 Å³ was calculated, containing 416 electrons. Graphical views were produced with Mercury. CCDC 1515333 (structure 1) and 1515335 (structure 2) contain the supplementary crystallographic data for this paper.

Theoretical Studies. Irppy-bpy, Irpiq-bpy, and Irpiq-L were studied by DFT^{50–53} and TD-DFT^{54–56} using Gaussian 09.⁵⁷ The B3LYP^{58–60} method and two basis sets (6-31G*⁶¹ for C and H and N/VDZ (valence double ζ) with the SBKJC effective core potential basis set^{62–65} for Ir) were used. Geometry optimizations were conducted without symmetry constraints. Frequency calculations on each optimized structure confirmed that energy minima had been reached in all cases. The energy, oscillator strength, and related MO contributions for the 100 lowest singlet–singlet and 10 lowest singlet–triplet excitations were obtained from the TD-DFT/singlets and TD-DFT/triplets output files, respectively, for the *S*₀-optimized geometry. GaussView5.09,⁶⁶ GaussSum3.0,⁶⁷ and Chemission4.43⁶⁸ were used for data analysis, visualization, and surface plots. All calculations were performed in a MeCN solution by using the polarized continuum solvation model, as implemented in Gaussian 09.^{69,70}

Setup of Gas Chromatography (GC). Monitoring of hydrogen evolution was performed with a PerkinElmer Clarus-480 gas chromatograph with a thermal conductivity detector, Ar as the carrier and eluent gases, a 7 ft. HayeSep N 60/80 precolumn, a 9 ft. molecular sieve 13 × 45/60 column, and a 2 mL injection loop. Three distinct solutions for the PS, catalyst and sacrificial donor and acid source [HBF_4 and 48% water or two solutions when Ir(III)–Co(III) dyads are used] were mixed together to obtain 5 mL of sample solutions in

standard 20 mL headspace vials. Those vials were placed on the LED panel in a thermostatic bath set at 20 °C. They were sealed with a rubber septum pierced with two stainless steel tubes. The first tube carried an Ar flow prebubbled into the solvent. The flow was set to 10 mL min⁻¹, adjusted with a manual flow controller (Porter 1000), and referenced with a digital flowmeter (PerkinElmer FlowMark). The second tube led the flow through a 2 mL overflow protection vial, then through an eight-port stream select valve (VICCI), and finally to the GC sample loop. A microprocessor (Arduino Uno) coupled with a custom PC interface allowed for timed injections. For a general calibration of hydrogen production, certified Ar stock cylinders at 500, 100, and 50 ppm of hydrogen were set to deliver a specific flow (inserted at the prebubbler to keep the vapor matrix consistent). The measured results, independent of the flow rate (under the same pressure), can easily be converted into the rate of hydrogen according to the following equation:

$$\text{H}_2 \text{ rate (}\mu\text{L min}^{-1}\text{)} = [\text{H}_2\text{standard}] \text{ (ppm)} \\ \times \text{Ar flow rate (mL min}^{-1}\text{)}$$

For a specific Ar flow, a syringe pump (New Era Pump) equipped with a gastight syringe (SGE) and a 26s gauge needle (Hamilton) was used to bubble different rates of 500 ppm H₂ in Ar gas into the sample, to a minimum of 0.1 mL min⁻¹. This gave a linear fit for the peak area of H₂ versus the flow rates of H₂ (see Figure S17)

Synthesis. 5-Bromo-2,2'-bipyridine was synthesized as previously described.⁷¹ Precursors [Ir(ppy)₂Cl]₂ and [Ir(piq)₂Cl]₂ were obtained according to Nonoyama's procedure.⁷² The Co(III) precursor Co(dmgH)(dmgH₂)Cl₂ was synthesized as previously described.⁷³ Irppy-bpy and Irpiq-bpy were synthesized according to the same procedure as that of Irpiq-L described below. All of the procedures applied to synthesize the Ir(III) PSs and Ir(III)-Co(III) dyad were performed in the dark under an Ar atmosphere.

2,2';5',4''-Terpyridine (L). To a Schlenk flask were successively added 5-bromo-2,2'-bipyridine (60.1 mg, 0.256 mmol), 1,2-dimethoxyethane (5.3 mL), water (0.7 mL), K₂CO₃ (72.9 mg, 0.528 mmol), and 4-pyridylboronic acid (42.3 mg, 0.344 mmol). The mixture was degassed and placed under Ar before [Pd(PPh₃)₄] (32.1 mg, 0.0278 mmol) was added. The reaction mixture was degassed again and refluxed for 4 days. The mixture was poured into water (30 mL). The solid was filtered on Celite and washed successively with water and ethyl acetate. The organic layer was separated, and the aqueous phase was extracted with ethyl acetate (3 × 30 mL). The organic layers were combined, dried over MgSO₄, and concentrated under reduced pressure. The product was purified by chromatography column on silica using 95/5 CH₂Cl₂/MeOH as the eluent. The fraction with R_f = 0.3 was collected and evaporated (*m* = 48.6 mg; -81.5%). ¹H NMR (CDCl₃): δ 8.97 (d, 1H, H-6', J_{6',4'} = 2.4 Hz, J_{6',3'} = 0.5 Hz), 8.73 (m, 3H, H-2'' + H-6'' + H-6), 8.55 (dd, H-3', J_{3',4'} = 8.3 Hz, J_{3',6'} = 0.5 Hz), 8.46 (dd, 1H, H-3, J₃₋₄ = 7.9 Hz, J₃₋₅ = 1.1 Hz), 8.08 (dd, 1H, H-4', J_{4',3'} = 8.3 Hz, J_{4',6'} = 2.4 Hz), 7.86 (dd, 1H, H-4, J₄₋₃ = 7.9 Hz, J₄₋₅ = 7.6 Hz, J₄₋₆ = 1.8 Hz), 7.60 (dd, 2H, H-3'' + H-5'', J_{3'',2'',16''} = 4.5 Hz, J_{5'',2'',16''} = 1.7 Hz), 7.36 (1H, ddd, H-5, J₅₋₄ = 7.6 Hz, J₅₋₆ = 4.8 Hz, J₅₋₃ = 1.1 Hz).

Irpiq-L. [Ir(piq)₂Cl]₂ (39.1 mg, 0.0307 mmol) and 2,2';5',4''-terpyridine (17.0 mg, 0.0729 mmol) were suspended in ethylene glycol (4.0 mL). The mixture was refluxed overnight. The solution was cooled to room temperature, and a saturated aqueous solution of NH₄PF₆ (5.0 mL) was added for precipitation. The solid was centrifuged, washed with water (3×), dried under reduced pressure, and washed again with diethyl ether (3×). HRMS (ESI). Calcd for [C₄₅H₃₁¹⁹³IrN₅-PF₆]⁺: *m/z* 832.21799. Found: *m/z* 834.21985. Calcd for [C₃₀H₂₀¹⁹³IrN₂-PF₆-L]⁺: *m/z* 601.12502. Found: *m/z* 601.12291. ¹H NMR (CD₃CN): δ 9.02 (m, 2H, H-f + H-f'), 8.65 (d, 1H, H-3', J_{3',4'} = 8.5 Hz), 8.59 (m, 3H, H-3 + H-2'' + H-6''), 8.41 (dd, 1H, H-4', J_{4',3'} = 8.5 Hz, J_{4',6'} = 2.2 Hz), 8.40 (m, 2H, H-g + H-g'), 8.14 (ddd, 1H, H-4, J₄₋₃ = 8.0 Hz, J₄₋₅ = 7.8 Hz, J₄₋₆ = 1.2 Hz), 7.99 (m, 2H, H-c + H-c'), 7.96 (d, 1H, H-6', J_{6',4'} = 2.2 Hz), 7.93 (dd, 1H, H-6, J₆₋₅ = 5.4 Hz, J₆₋₄ = 1.2 Hz), 7.83 (m, 4H, H-d + H-d' + H-e + H-e'), 7.57 (m, 2H, H-a/b + H-a'/b'), 7.50 (ddd, 1H, H-5, J₅₋₄ = 7.8 Hz, J₅₋₆ =

5.4 Hz, J₅₋₃ = 0.6 Hz), 7.43 (m, 2H, H-b/a + H-b'/a'), 7.24 (dd, 2H, H-3'' + H-5'', J_{3'',2'',16''} = 4.5 Hz, J_{5'',2'',16''} = 1.7 Hz), 7.16 (m, 2H, H-h + H-h'), 6.91 (m, 2H, H-i + H-i'), 6.34 (m, 2H, H-j + H-j').

Irpiq-L-Co. To a suspension of Co(dmgH)(dmgH₂)Cl₂ (6.6 mg, 0.0183 mmol) in methanol (2.5 mL) was added Et₃N (2.4 μL, 0.0172 mmol). The mixture was stirred at room temperature for 15 min until a brown solution was obtained. A solution of Irpiq-L (16.8 mg, 0.0172 mmol) in dichloromethane (2.5 mL) was slowly added to this solution, and the mixture was stirred at room temperature for 1 h 30 min. A stream of air was passed through the solution for 15 min, and diethyl ether was added for precipitation. The orange precipitate was centrifuged and washed with diethyl ether. The product was dissolved in acetone to remove impurities. The crude product was purified by column chromatography on SiO₂ (95/5 CH₂Cl₂/MeOH). HRMS (ESI). Calcd for [C₅₃H₄₅³⁷Cl⁵⁹Co¹⁹³IrN₉O₄-PF₆]⁺: *m/z* 1158.22388. Found: *m/z* 1158.22415. Calcd for [C₄₅H₃₁¹⁹³IrN₅-PF₆-Co-(dmgH)₂Cl]⁺: *m/z* 834.22032. Found: *m/z* 834.22024. ¹H NMR (acetone-*d*₆): δ 9.10 (m, 2H, H-f + H-f'), 9.03 (d, 1H, H-3', J_{3',4'} = 8.6 Hz), 8.96 (d, 1H, H-3, J₃₋₄ = 8.1 Hz), 8.66 (dd, 1H, H-4', J_{4',3'} = 8.6 Hz, J_{4',6'} = 2.0 Hz), 8.45 (m, 2H, H-g + H-g'), 8.32 (ddd, 1H, H-4, J₄₋₃ = 8.1 Hz, J₄₋₅ = 8.0 Hz, J₄₋₆ = 1.5 Hz), 8.17 (dd, 2H, H-2'' + H-6'', J_{2'',16'',3'',15''} = 5.6 Hz, J_{2'',16'',5'',13''} = 1.4 Hz), 8.13 (d, 1H, H-6', J_{6',4'} = 2.0 Hz), 8.05 (m, 3H, H-6 + H-c + H-c'), 7.92 (m, 4H, H-d + H-d' + H-e + H-e'), 7.75 (m, 3H, H-5 + H-a/b + H-a'/b'), 7.54 (m, 2H, H-b/a + H-b'/a'), 7.42 (dd, 2H, H-3'' + H-5'', J_{3'',2'',16''} = 5.6 Hz, J_{5'',2'',16''} = 1.4 Hz), 7.18 (m, 2H, H-h + H-h'), 6.94 (m, 2H, H-i + H-i'), 6.39 (m, 2H, H-j + H-j'), 2.30 (s, 12H, -CH₃dmgH).

■ ASSOCIATED CONTENT

📄 Supporting Information

The Supporting Information is available free of charge on the ACS Publications website at DOI: 10.1021/acs.inorgchem.7b00684.

Experimental details, synthesis of the Ir(III)-based compounds, cyclic voltammetry, hydrogen photoproduction, and TD-DFT calculations (PDF)

Accession Codes

CCDC 1515333 and 1515335 and contain the supplementary crystallographic data for this paper. These data can be obtained free of charge via www.ccdc.cam.ac.uk/data_request/cif, or by emailing data_request@ccdc.cam.ac.uk, or by contacting The Cambridge Crystallographic Data Centre, 12, Union Road, Cambridge CB2 1EZ, UK; fax: +44 1223 336033.

■ AUTHOR INFORMATION

Corresponding Authors

*E-mail: garry.hanan@umontreal.ca.

*E-mail: benjamin.elias@uclouvain.be.

ORCID

Cédric Lentz: 0000-0001-9741-686X

Thomas Auvray: 0000-0003-4340-2555

Author Contributions

The manuscript was written through contributions of all authors.

Notes

The authors declare no competing financial interest.

■ ACKNOWLEDGMENTS

C.L. and B.E. gratefully acknowledge the Région Wallonne, Belgium, the Université catholique de Louvain, Belgium, and the Prix Pierre et Colette Bauchau, Belgium, for financial support. G.H. thanks the Natural Sciences and Engineering Research Council, Canada, and the Direction des Affaires Internationales de l'Université de Montréal, Canada, for

financial support. Prof. K. Van Hecke is thanked for allowing access to his diffractometer. B.E. and G.H. thank the Wallonie Bruxelles International program for travel grants.

REFERENCES

- (1) Han, Z.; Eisenberg, R. Fuel from water: the photochemical generation of hydrogen from water. *Acc. Chem. Res.* **2014**, *47*, 2537–2544.
- (2) Pagliaro, M.; Konstandopoulos, A. G.; Ciriminna, R.; Palmisano, G. Solar hydrogen: fuel of the near future. *Energy Environ. Sci.* **2010**, *3*, 279–287.
- (3) Pellow, M. A.; Emmott, C. J. M.; Barnhart, C. J.; Benson, S. M. Hydrogen or batteries for grid storage? A net energy analysis. *Energy Environ. Sci.* **2015**, *8*, 1938–1952.
- (4) Berardi, S.; Drouet, S.; Francas, L.; Gimbert-Surinach, C.; Guttentag, M.; Richmond, C.; Stoll, T.; Llobet, A. Molecular artificial photosynthesis. *Chem. Soc. Rev.* **2014**, *43*, 7501–7519.
- (5) Queyriaux, N.; Jane, R. T.; Massin, J.; Artero, V.; Chavarot-Kerlidou, M. Recent Developments in Hydrogen Evolving Molecular Cobalt(II)-Polypyridyl Catalysts. *Coord. Chem. Rev.* **2015**, *304–305*, 3–19.
- (6) Willkomm, J.; Orchard, K. L.; Reynal, A.; Pastor, E.; Durrant, J. R.; Reisner, E. Dye-sensitized semiconductors modified with molecular catalysts for light-driven H₂ production. *Chem. Soc. Rev.* **2016**, *45*, 9–23.
- (7) Armaroli, N.; Balzani, V. The hydrogen issue. *ChemSusChem* **2011**, *4*, 21–36.
- (8) Balzani, V.; Credi, A.; Venturi, M. Photochemical conversion of solar energy. *ChemSusChem* **2008**, *1*, 26–58.
- (9) Natali, M.; Argazzi, R.; Chiorboli, C.; Iengo, E.; Scandola, F. Photocatalytic hydrogen evolution with a self-assembling reductant-sensitizer-catalyst system. *Chem. - Eur. J.* **2013**, *19*, 9261–9271.
- (10) Teets, T. S.; Nocera, D. G. Photocatalytic hydrogen production. *Chem. Commun.* **2011**, *47*, 9268–9274.
- (11) Mulfort, K. L.; Utschig, L. M. Modular Homogeneous Chromophore-Catalyst Assemblies. *Acc. Chem. Res.* **2016**, *49*, 835–843.
- (12) Arrigo, A.; Santoro, A.; Indelli, M. T.; Natali, M.; Scandola, F.; Campagna, S. On the effect of the nature of the bridge on oxidative or reductive photoinduced electron transfer in donor-bridge-acceptor systems. *Phys. Chem. Chem. Phys.* **2014**, *16*, 818–826.
- (13) Eckenhoff, W. T.; Eisenberg, R. Molecular systems for light driven hydrogen production. *Dalton Trans.* **2012**, *41*, 13004–13021.
- (14) Fihri, A.; Artero, V.; Pereira, A.; Fontecave, M. Efficient H₂-producing photocatalytic systems based on cyclometalated iridium- and tricarbonylrhenium-diimine photosensitizers and cobaloxime catalysts. *Dalton Trans.* **2008**, 5567–5569.
- (15) Li, C.; Wang, M.; Pan, J.; Zhang, P.; Zhang, R.; Sun, L. Photochemical hydrogen production catalyzed by polypyridyl ruthenium–cobaloxime heterobinuclear complexes with different bridges. *J. Organomet. Chem.* **2009**, *694*, 2814–2819.
- (16) DiSalle, B. F.; Bernhard, S. Orchestrated photocatalytic water reduction using surface-adsorbing iridium photosensitizers. *J. Am. Chem. Soc.* **2011**, *133*, 11819–11821.
- (17) Karnahl, M.; Kuhnt, C.; Heinemann, F. W.; Schmitt, M.; Rau, S.; Popp, J.; Dietzek, B. Synthesis and photophysics of a novel photocatalyst for hydrogen production based on a tetrapyrrodoacridine bridging ligand. *Chem. Phys.* **2012**, *393*, 65–73.
- (18) Kowacs, T.; O'Reilly, L.; Pan, Q.; Huijser, A.; Lang, P.; Rau, S.; Browne, W. R.; Pryce, M. T.; Vos, J. G. Subtle Changes to Peripheral Ligands Enable High Turnover Numbers for Photocatalytic Hydrogen Generation with Supramolecular Photocatalysts. *Inorg. Chem.* **2016**, *55*, 2685–2690.
- (19) Kowacs, T.; Pan, Q.; Lang, P.; O'Reilly, L.; Rau, S.; Browne, W. R.; Pryce, M. T.; Huijser, A.; Vos, J. G. Supramolecular bimetallic assemblies for photocatalytic hydrogen generation from water. *Faraday Discuss.* **2015**, *185*, 143–170.
- (20) Arachchige, S. M.; Brown, J. R.; Chang, E.; Jain, A.; Zigler, D. F.; Rangan, K.; Brewer, K. J. Design considerations for a system for photocatalytic hydrogen production from water employing mixed-metal photochemical molecular devices for photoinitiated electron collection. *Inorg. Chem.* **2009**, *48*, 1989–2000.
- (21) Elvington, M.; Brown, J.; Arachchige, S. M.; Brewer, K. J. Photocatalytic hydrogen production from water employing a Ru, Rh, Ru molecular device for photoinitiated electron collection. *J. Am. Chem. Soc.* **2007**, *129*, 10644–10645.
- (22) Ozawa, H.; Sakai, K. Photo-hydrogen-evolving molecular devices driving visible-light-induced water reduction into molecular hydrogen: structure-activity relationship and reaction mechanism. *Chem. Commun.* **2011**, *47*, 2227–2242.
- (23) Ozawa, H.; Sakai, K. An Effect of Structural Modification in the Photo-hydrogen-evolving RuII/III Dimers. *Chem. Lett.* **2007**, *36*, 920–921.
- (24) Sakai, K.; Ozawa, H. Homogeneous catalysis of platinum(II) complexes in photochemical hydrogen production from water. *Coord. Chem. Rev.* **2007**, *251*, 2753–2766.
- (25) Stoll, T.; Castillo, C. E.; Kayanuma, M.; Sandroni, M.; Daniel, C.; Odobel, F.; Fortage, J.; Collomb, M.-N. Photo-induced redox catalysis for proton reduction to hydrogen with homogeneous molecular systems using rhodium-based catalysts. *Coord. Chem. Rev.* **2015**, *304–305*, 20–37.
- (26) Zarkadoulas, A.; Koutsouri, E.; Kefalidi, C.; Mitsopoulou, C. A. Rhenium complexes in homogeneous hydrogen evolution. *Coord. Chem. Rev.* **2015**, *304–305*, 55–72.
- (27) Ozawa, H.; Yokoyama, Y.; Haga, M. A.; Sakai, K. Syntheses, characterization, and photo-hydrogen-evolving properties of tris(2,2'-bipyridine)ruthenium(II) derivatives tethered to a cis-Pt(II)Cl₂ unit: insights into the structure-activity relationship. *Dalton Trans.* **2007**, 1197–1206.
- (28) Radhakrishnan, A. N.; Rao, P. P.; Linsa, K. S.; Deepa, M.; Koshy, P. Influence of disorder-to-order transition on lattice thermal expansion and oxide ion conductivity in (Ca_xGd_{1-x})(₂)(Zr_{1-x}M_x)₂O₇ pyrochlore solid solutions. *Dalton Trans.* **2011**, *40*, 3839–3848.
- (29) Porras, J. A.; Mills, I. N.; Transue, W. J.; Bernhard, S. Highly Fluorinated Ir(III)-2,2':6',2''-Terpyridine-Phenylpyridine-X Complexes via Selective C-F Activation: Robust Photocatalysts for Solar Fuel Generation and Photoredox Catalysis. *J. Am. Chem. Soc.* **2016**, *138*, 9460–9472.
- (30) Fan, S.; Zong, X.; Shaw, P. E.; Wang, X.; Geng, Y.; Smith, A. R.; Burn, P. L.; Wang, L.; Lo, S. C. Energetic requirements of iridium(III) complex based photosensitizers in photocatalytic hydrogen generation. *Phys. Chem. Chem. Phys.* **2014**, *16*, 21577–21585.
- (31) Kaefter, N.; Chavarot-Kerlidou, M.; Artero, V. Hydrogen evolution catalyzed by cobalt diimine-dioxime complexes. *Acc. Chem. Res.* **2015**, *48*, 1286–1295.
- (32) Artero, V.; Chavarot-Kerlidou, M.; Fontecave, M. Splitting water with cobalt. *Angew. Chem., Int. Ed.* **2011**, *50*, 7238–7266.
- (33) Jacques, A.; Schott, O.; Robeyns, K.; Hanan, G. S.; Elias, B. Hydrogen Photoevolution from a Green-Absorbing Iridium(III)-Cobalt(III) Dyad. *Eur. J. Inorg. Chem.* **2016**, *2016*, 1779–1783.
- (34) Rousset, E.; Chartrand, D.; Ciofini, I.; Marvaud, V.; Hanan, G. S. Red-light-driven photocatalytic hydrogen evolution using a ruthenium quaterpyridine complex. *Chem. Commun.* **2015**, *51*, 9261–9264.
- (35) Sabatini, R. P.; Lindley, B.; McCormick, T. M.; Lazarides, T.; Brennessel, W. W.; McCamant, D. W.; Eisenberg, R. Efficient Bimolecular Mechanism of Photochemical Hydrogen Production Using Halogenated Boron-Dipyromethene (Bodipy) Dyes and a Bis(dimethylglyoxime) Cobalt(III) Complex. *J. Phys. Chem. B* **2016**, *120*, 527–534.
- (36) Manton, J. C.; Long, C.; Vos, J. G.; Pryce, M. T. Porphyrin-cobaloxime complexes for hydrogen production, a photo- and electrochemical study, coupled with quantum chemical calculations. *Dalton Trans.* **2014**, *43*, 3576–3583.
- (37) Peuntinger, K.; Lazarides, T.; Dafnomili, D.; Charalambidis, G.; Landrou, G.; Kahnt, A.; Sabatini, R. P.; McCamant, D. W.; Gryko, D.

- T.; Coutsolelos, A. G.; Guldi, D. M. Photoinduced Charge Transfer in Porphyrin–Cobaloxime and Corrole–Cobaloxime Hybrids. *J. Phys. Chem. C* **2013**, *117*, 1647–1655.
- (38) Costa, R. n. D.; Ortá, E.; Bolink, H. J.; Graber, S.; Schaffner, S.; Neuburger, M.; Housecroft, C. E.; Constable, E. C. Archetype Cationic Iridium Complexes and Their Use in Solid-State Light-Emitting Electrochemical Cells. *Adv. Funct. Mater.* **2009**, *19*, 3456–3463.
- (39) Liu, S.-J.; Zhao, Q.; Fan, Q.-L.; Huang, W. A Series of Red-Light-Emitting Ionic Iridium Complexes: Structures, Excited State Properties, and Application in Electroluminescent Devices. *Eur. J. Inorg. Chem.* **2008**, *2008*, 2177–2185.
- (40) Panagiotopoulos, A.; Ladomenou, K.; Sun, D.; Artero, V.; Coutsolelos, A. G. Photochemical hydrogen production and cobaloximes: the influence of the cobalt axial N-ligand on the system stability. *Dalton Trans.* **2016**, *45*, 6732–6738.
- (41) Du, P.; Schneider, J.; Luo, G.; Brennessel, W. W.; Eisenberg, R. Visible light-driven hydrogen production from aqueous protons catalyzed by molecular cobaloxime catalysts. *Inorg. Chem.* **2009**, *48*, 4952–4962.
- (42) Zhao, Q.; Liu, S.; Shi, M.; Wang, C.; Yu, M.; Li, L.; Li, F.; Yi, T.; Huang, C. Series of new cationic iridium(III) complexes with tunable emission wavelength and excited state properties: structures, theoretical calculations, and photophysical and electrochemical properties. *Inorg. Chem.* **2006**, *45*, 6152–6160.
- (43) Lawrence, M. A.; Celestine, M. J.; Artis, E. T.; Joseph, L. S.; Esquivel, D. L.; Ledbetter, A. J.; Crokek, D. M.; Jarrett, W. L.; Bayse, C. A.; Brewer, M. I.; Holder, A. A. Computational, electrochemical, and spectroscopic studies of two mononuclear cobaloximes: the influence of an axial pyridine and solvent on the redox behaviour and evidence for pyridine coordination to cobalt(i) and cobalt(ii) metal centres. *Dalton Trans.* **2016**, *45*, 10326–10342.
- (44) Ozawa, H.; Haga, M. A.; Sakai, K. A photo-hydrogen-evolving molecular device driving visible-light-induced EDTA-reduction of water into molecular hydrogen. *J. Am. Chem. Soc.* **2006**, *128*, 4926–4927.
- (45) Schulz, M.; Karnahl, M.; Schwalbe, M.; Vos, J. G. The role of the bridging ligand in photocatalytic supramolecular assemblies for the reduction of protons and carbon dioxide. *Coord. Chem. Rev.* **2012**, *256*, 1682–1705.
- (46) Deponti, E.; Natali, M. Photocatalytic hydrogen evolution with ruthenium polypyridine sensitizers: unveiling the key factors to improve efficiencies. *Dalton Trans.* **2016**, *45*, 9136–9147.
- (47) Sheldrick, G. M. A short history of SHELX. *Acta Crystallogr., Sect. A: Found. Crystallogr.* **2008**, *64*, 112–122.
- (48) Sheldrick, G. M. SHELXT - integrated space-group and crystal-structure determination. *Acta Crystallogr., Sect. A: Found. Adv.* **2015**, *71*, 3–8.
- (49) Spek, A. L. Structure validation in chemical crystallography. *Acta Crystallogr., Sect. D: Biol. Crystallogr.* **2009**, *65*, 148–155.
- (50) Parr, R. G.; Weitao, Y. *Density-Functional Theory of Atoms and Molecules*; Oxford University Press, 1994.
- (51) Salahub, D. R.; Zerner, M. C. *The Challenge of d and f Electrons*; ACS Symposium Series 394; American Chemical Society, 1989.
- (52) Hohenberg, P.; Kohn, W. Inhomogeneous Electron Gas. *Phys. Rev.* **1964**, *136*, B864–B871.
- (53) Kohn, W.; Sham, L. J. Self-Consistent Equations Including Exchange and Correlation Effects. *Phys. Rev.* **1965**, *140*, A1133–A1138.
- (54) Bauernschmitt, R.; Ahlrichs, R. Treatment of electronic excitations within the adiabatic approximation of time dependent density functional theory. *Chem. Phys. Lett.* **1996**, *256*, 454–464.
- (55) Casida, M. E.; Jamorski, C.; Casida, K. C.; Salahub, D. R. Molecular excitation energies to high-lying bound states from time-dependent density-functional response theory: Characterization and correction of the time-dependent local density approximation ionization threshold. *J. Chem. Phys.* **1998**, *108*, 4439–4449.
- (56) Stratmann, R. E.; Scuseria, G. E.; Frisch, M. J. An efficient implementation of time-dependent density-functional theory for the calculation of excitation energies of large molecules. *J. Chem. Phys.* **1998**, *109*, 8218–8224.
- (57) Frisch, M. J.; Trucks, G. W.; Schlegel, H. B.; Scuseria, G. E.; Robb, M. A.; Cheeseman, J. R.; Scalmani, G.; Barone, V.; Mennucci, B.; Petersson, G. A.; Nakatsuji, H.; Caricato, M.; Li, X.; Hratchian, H. P.; Izmaylov, A. F.; Bloino, J.; Zheng, G.; Sonnenberg, J. L.; Hada, M.; Ehara, M.; Toyota, K.; Fukuda, R.; Hasegawa, J.; Ishida, M.; Nakajima, T.; Honda, Y.; Kitao, O.; Nakai, H.; Vreven, T.; Montgomery, J. A., Jr.; Peralta, J. E.; Ogliaro, F.; Bearpark, M. J.; Heyd, J. J.; Brothers, E. N.; Kudin, K. N.; Staroverov, V. N.; Kobayashi, R.; Normand, J.; Raghavachari, K.; Rendell, A. P.; Burant, J. C.; Iyengar, S. S.; Tomasi, J.; Cossi, M.; Rega, N.; Millam, J. M.; Klene, M.; Knox, J. E.; Cross, J. B.; Bakken, V.; Adamo, C.; Jaramillo, J.; Gomperts, R.; Stratmann, R. E.; Yazyev, O.; Austin, A. J.; Cammi, R.; Pomelli, C.; Ochterski, J. W.; Martin, R. L.; Morokuma, K.; Zakrzewski, V. G.; Voth, G. A.; Salvador, P.; Dannenberg, J. J.; Dapprich, S.; Daniels, A. D.; Farkas, O.; Foresman, J. B.; Ortiz, J. V.; Cioslowski, J.; Fox, D. J. *Gaussian 09*, revision E.01; Gaussian, Inc.: Wallingford, CT, 2009.
- (58) Miehlich, B.; Savin, A.; Stoll, H.; Preuss, H. Results obtained with the correlation energy density functionals of Becke and Lee, Yang and Parr. *Chem. Phys. Lett.* **1989**, *157*, 200–206.
- (59) Becke, A. D. Density-functional thermochemistry. III. The role of exact exchange. *J. Chem. Phys.* **1993**, *98*, 5648–5652.
- (60) Lee, C.; Yang, W.; Parr, R. G. Development of the Colle-Salvetti correlation-energy formula into a functional of the electron density. *Phys. Rev. B: Condens. Matter Mater. Phys.* **1988**, *37*, 785–789.
- (61) Mitin, A. V.; Baker, J.; Pulay, P. An improved 6-31G* basis set for first-row transition metals. *J. Chem. Phys.* **2003**, *118*, 7775–7782.
- (62) Stevens, W. J.; Krauss, M.; Basch, H.; Jasien, P. G. Relativistic compact effective potentials and efficient, shared-exponent basis sets for the third-, fourth-, and fifth-row atoms. *Can. J. Chem.* **1992**, *70*, 612–630.
- (63) Cundari, T. R.; Stevens, W. J. Effective core potential methods for the lanthanides. *J. Chem. Phys.* **1993**, *98*, 5555–5565.
- (64) Stevens, W. J.; Basch, H.; Krauss, M. Compact effective potentials and efficient shared-exponent basis sets for the first- and second-row atoms. *J. Chem. Phys.* **1984**, *81*, 6026–6033.
- (65) Binkley, J. S.; Pople, J. A.; Hehre, W. J. Self-consistent molecular orbital methods. 21. Small split-valence basis sets for first-row elements. *J. Am. Chem. Soc.* **1980**, *102*, 939–947.
- (66) Dennington, R.; Keith, J. A.; Millam, J. M. *GaussView*, version 5.09; Gaussian Inc.: Shawnee Mission, KS, 2009.
- (67) O'Boyle, N. M.; Tenderholt, A. L.; Langner, K. M. cclib: a library for package-independent computational chemistry algorithms. *J. Comput. Chem.* **2008**, *29*, 839–845.
- (68) Skripnikov, L. *Chemissian*, version 4.43; Chemissian, 2005–2016.
- (69) Miertuš, S.; Scrocco, E.; Tomasi, J. Electrostatic interaction of a solute with a continuum. A direct utilization of AB initio molecular potentials for the prevision of solvent effects. *Chem. Phys.* **1981**, *55*, 117–129.
- (70) Tomasi, J.; Mennucci, B.; Cammi, R. Quantum mechanical continuum solvation models. *Chem. Rev.* **2005**, *105*, 2999–3093.
- (71) Brotschi, C.; Mathis, G.; Leumann, C. J. Bipyrindyl- and biphenyl-DNA: a recognition motif based on interstrand aromatic stacking. *Chem. - Eur. J.* **2005**, *11*, 1911–1923.
- (72) Nonoyama, M. Benzo[h]quinolin-10-yl-Niridium(III) Complexes. *Bull. Chem. Soc. Jpn.* **1974**, *47*, 767–768.
- (73) Trogler, W. C.; Stewart, R. C.; Epps, L. A.; Marzilli, L. G. Cis and trans effects on the proton magnetic resonance spectra of cobaloximes. *Inorg. Chem.* **1974**, *13*, 1564–1570.